Hindawi
Journal of Advanced Transportation
Volume 2019, Article ID 1813763, 9 pages
https://doi.org/10.1155/2019/1813763

Research Article

Automatic Segmentation and Enhancement of Pavement Cracks Based on 3D Pavement Images

Baoxian Li[1], **Kelvin C. P. Wang**[1,2], **Allen Zhang**[2], **Yue Fei**[2] **and Giuseppe Sollazzo**[3]

[1]*School of Civil and Environmental Engineering, Southwest Jiaotong University, Chengdu 610031, China*
[2]*School of Civil and Environmental Engineering, Oklahoma State University, Stillwater, OK 74078, USA*
[3]*Department of Engineering, University of Messina Vill. S. Agata, C.da di Dio, 98166 Messina, Italy*

Correspondence should be addressed to Allen Zhang; allen.zhang@okstate.edu

Received 19 January 2018; Revised 7 November 2018; Accepted 15 January 2019; Published 18 February 2019

Academic Editor: Aboelmaged Noureldin

Pavement cracking is a significant symptom of pavement deterioration and deficiency. Conventional manual inspections of road condition are gradually replaced by novel automated inspection systems. As a result, a great amount of pavement surface information is digitized by these systems with a high resolution. With pavement surface data, pavement cracks can be detected using crack detection algorithms. In this paper, a fully automated algorithm for segmenting and enhancing pavement crack is proposed, which consists of four major procedures. First, a preprocessing procedure is employed to remove spurious noise and rectify the original 3D pavement data. Second, crack saliency maps are segmented from 3D pavement data using steerable matched filter bank. Third, 2D tensor voting is applied to crack saliency maps to achieve better curve continuity of crack structure and higher accuracy. Finally, postprocessing procedures are used to remove redundant noises. The proposed procedures were evaluated over 200 asphalt pavement images with diverse cracks. The experimental results demonstrated that the proposed method showed a high performance and could achieve average precision of 88.38%, recall of 93.15%, and F-measure of 90.68%, respectively. Accordingly, the proposed approach can be helpful in automated pavement condition assessment.

1. Introduction

Effective and efficient pavement condition assessment is crucial for determining pavement maintenance schedules, evaluating performance, planning rehabilitation, etc. Because pavement cracking is an important indicator of pavement deterioration and deficiency, it is widely considered as an integral part of regional pavement distress surveys [1]. Many studies show that timely and accurately inspected pavement cracks can help transportation agencies reduce road maintenance cost and extend pavement service life [2, 3].

In some developing countries, pavements are mainly investigated by human inspectors [4]. The traditional manual pavement inspection is unsafe, time-consuming, expensive, and subjective. Hence, the automation in pavement inspection and evaluation has become increasingly popular and dominant [5]. There are two types of imaging techniques extensively adopted in automated pavement data collection: two-dimensional (2D) imaging technologies and three-dimension (3D) imaging technologies. The early 2D imaging based pavement detection systems [6, 7] were developed by integrating hardware such as line-scan cameras, laser illumination systems and other auxiliary equipment. With the emergence of advanced technologies such as high-speed and high-resolution 3D industry cameras, the pavement inspection methods based on 3D scanning have attracted more and more interests for the following reasons:

(1) The surface information in 3D images collected by advanced data acquisition systems is more accurate than those in 2D images. Figure 1 shows a comparison between 2D and 3D pavement images. The 2D images collected in gray-scale formats have limited data range, while the 3D images are able to represent the actual depths of pavement surfaces.

(2) 3D pavement images have higher quality than 2D pavement images. Due to their different imaging principles, 3D pavement images are less prone to noise related to oil stains, dark shadows, tire marks, etc. [8, 9].

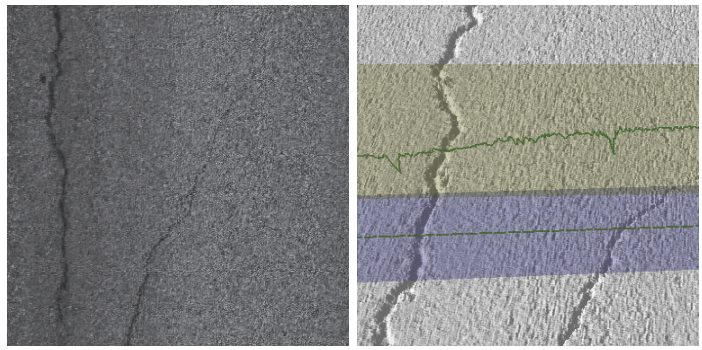

Figure 1: The 2D pavement image (left) and 3D pavement image (right): the up green line is the transverse profile of a patch of pavement surface.

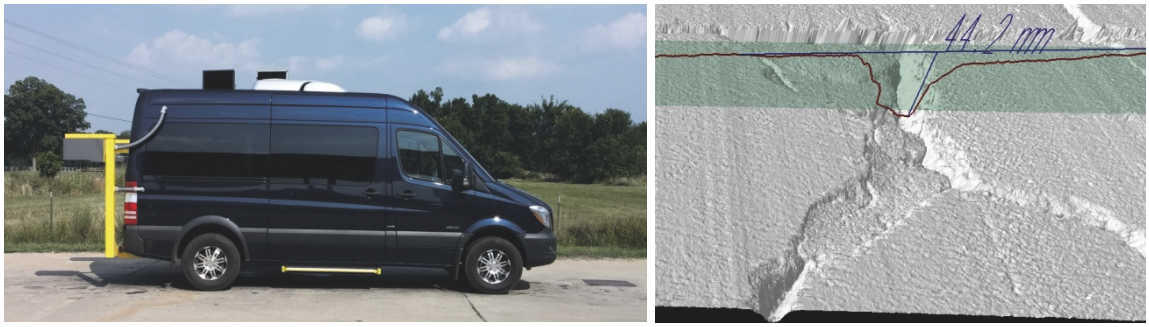

Figure 2: *PaveVision3D* Ultra System (left) and representative 3D pavement data (right).

(3) The depth information collected by 3D techniques is more helpful in analyzing cracks, textures, rutting, etc. [10–12].

Due to recent developments and innovations in hardware devices, laser line-scanning based techniques tend to become mature enough for high-resolution 3D pavement data collection. Laurent et al. [13] developed a Laser Crack Measurement System (LCMS) composed of two laser profilers to acquire high-resolution 3D road surface data. Moreno et al. [14] proposed an electric vehicle equipped with a laser scanner to achieve high density of surveyed points. Furthermore, the *PaveVision3D* System mounted on Digital Highway Data Vehicle (DHDV) (Figure 2) is able to obtain full-lane-scale 3D data in 1-mm resolution at a highway speed up to 100 km/h no matter during night- or day-time [15, 16].

Although automation in pavement data collection has achieved remarkable progress, automated distress detection still faces great challenge due to the complexity and diversity of pavement surfaces [17, 18]. As a major task of distress survey, automated crack detection has been studied for a long time. Intensity-thresholding methods have been proposed to transform the pavement images into a binary domain such that the pavement distresses are easier to be recognized [19, 20]. However, those methods fail to handle images with unevenly distributed illuminance. Edge detection based methods, such as morphological filters [21] and BEMD [22], are also introduced for pavement crack detection. Nevertheless, those methods tend to generate discontinuous or nonintegral cracks. Wavelet-based approaches [23] have been utilized to decompose the original data into different frequency subbands. Unfortunately, those approaches have limitations in detecting discontinuous or high-curvature cracks. Currently, there are some successful applications of machine learning techniques, such as Artificial Neural Network (ANN) and Support Vector Machine (SVM), in classifying cracks on pavement surface [24].

In rest of this paper, firstly, the proposed method is explained in detail. Secondly, an image library of 200 pavement 3D data verifies the accuracy and effectiveness of the proposed method. Lastly, discussion and conclusions are given, respectively.

2. Methodology

In this paper, all the testing and validation data are 3D pavement images collected by *PaveVision3D* System. Each 3D image in size of 2048 × 4096 is able to cover roughly 2 × 4 m^2 surface area with 1 mm resolution. As shown in Figure 3, the proposed method represents the following procedures: (1) Preprocessing techniques are utilized to remove noises and to rectify pavement data. (2) Steerable Matched Filter Bank (SMFB) is applied on 3D pavement data for segmenting crack saliency maps. (3) 2D Tensor Voting is used to enhance the crack continuity based on the crack saliency maps. (4) Postprocessing is conducted to remove false-positive errors.

2.1. Spurious Noise Removal and 3D Pavement Data Rectification. 3D pavement data may have noises caused by invalid laser points and vehicle vibration or movement. Therefore, spurious noises removal and pavement 3D data rectification

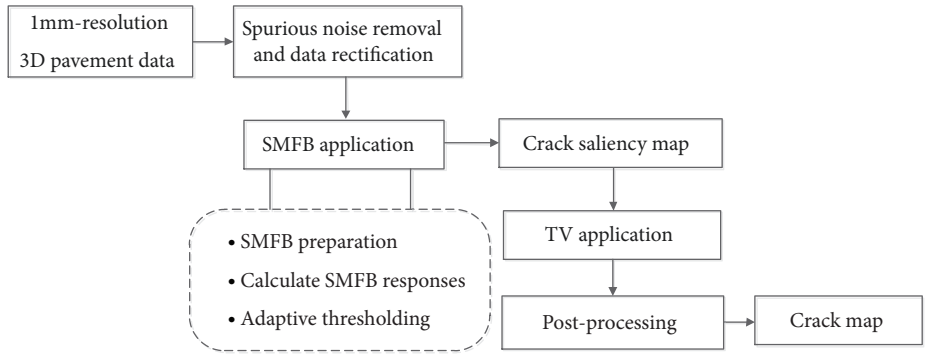

Figure 3: Flowchart of the proposed method.

are needed at the first stage. A typical 2D Gaussian filter with standard deviation σ is used for noise removal. Equation (1) gives each value of the 2D Gaussian filter at position $p_0 = (x, y)$.

$$g(p_0; \sigma) = \frac{1}{\sqrt{2\pi}\sigma} e^{-(x^2+y^2)/2\sigma^2} \quad (1)$$

In this case, the size of the filter is 3×3, and σ is equal to 2. In order to determine the presence of a spurious noise at each point (x, y), the following criterion is conducted:

$$Value'(x, y) = \begin{cases} FValue(x, y) & if\ abs[Value(x, y) - FValue(x, y)] > thres \\ Value(x, y) & otherwise \end{cases} \quad (2)$$

where $Value(x, y)$ is the original pixel value at the point (x, y), $FValue(x, y)$ is the filtered pixel value at the point (x, y), and *thres* is a given threshold.

After obtaining $Value'(x, y)$, another big-size 2D Gaussian filter is applied to smooth the entire image. In this case, the filter size is 101×101, and σ is equal to 80. Let $FValue'(x, y)$ be the convolved images based on $Value'(x, y)$; then the rectified image will be

$$RValue'(x, y) = FValue'(x, y) - Value'(x, y) \quad (3)$$

where $RValue'$ is the rectified pixel value at the point (x, y); $FValue'$ is the convolved pixel value at the point (x, y).

Figure 4 shows sample profiles in both transverse and longitudinal directions. The top images (a) and (b) show the original pavement profile. The bottom images (c) and (d) illustrate rectified profiles based on (3). The red lines are their smoothed profile.

2.2. Steerable Matched Filter Bank (SMFB). The steerable filter introduced by Freeman and Adelson [25] is a linear combination of a few basic filters. Particularly, steerable filter is popular in crack and ridge detection due to high efficiency [26–28]. In this study, the SMFB method uses second-derivative Gaussians as basic filters. Equation (1) gives the 2D Gaussian with variance σ, and (4) gives its second derivatives. Equation (5) shows the formulation of the filter $f(\sigma, \theta)$, where $\theta \in [-\pi/2, \pi/2]$ is the orientation of the filter:

$$g_{xx}(x, y) = \frac{\left(x^2 - \sigma^2\right) e^{-(x^2+y^2)/2\sigma^2}}{\sqrt{2\pi}\sigma^5}$$

$$g_{yy}(x, y) = \frac{\left(y^2 - \sigma^2\right) e^{-(x^2+y^2)/2\sigma^2}}{\sqrt{2\pi}\sigma^5} \quad (4)$$

$$g_{xy}(x, y) = g_{yx}(x, y) = \frac{xye^{-(x^2+y^2)/2\sigma^2}}{\sqrt{2\pi}\sigma^5}$$

$$f(\sigma, \theta) = g_{xx}\cos^2\theta + 2g_{xy}\cos\theta\sin\theta + g_{yy}\sin^2\theta \quad (5)$$

A filter bank is generated by using Steerable Matched Filter, namely SMFB. Table 1 lists 52 components of SMFB with different parameters, filter size, σ, and θ. Four different σ are assigned to consider the varying widths of cracks. The orientations are incremented with a fix angle interval 15° to capture crack segments in varying orientations. In order to yield nearly zero responses within noncrack area, the filters are shifted to have a zero mean. All filters in SMFB are illustrated in Figure 5.

Each preprocessed 3D pavement image is convolved with all 52 filters in SMFB. At each pixel, only the maximum convolutional response is preserved as a result of SMFB operation. Mathematically, (6)~(8) give the specific calculation procedures.

$$r_i(p; \sigma, \theta) = k_i(\sigma, \theta) \otimes V(p) \quad (6)$$

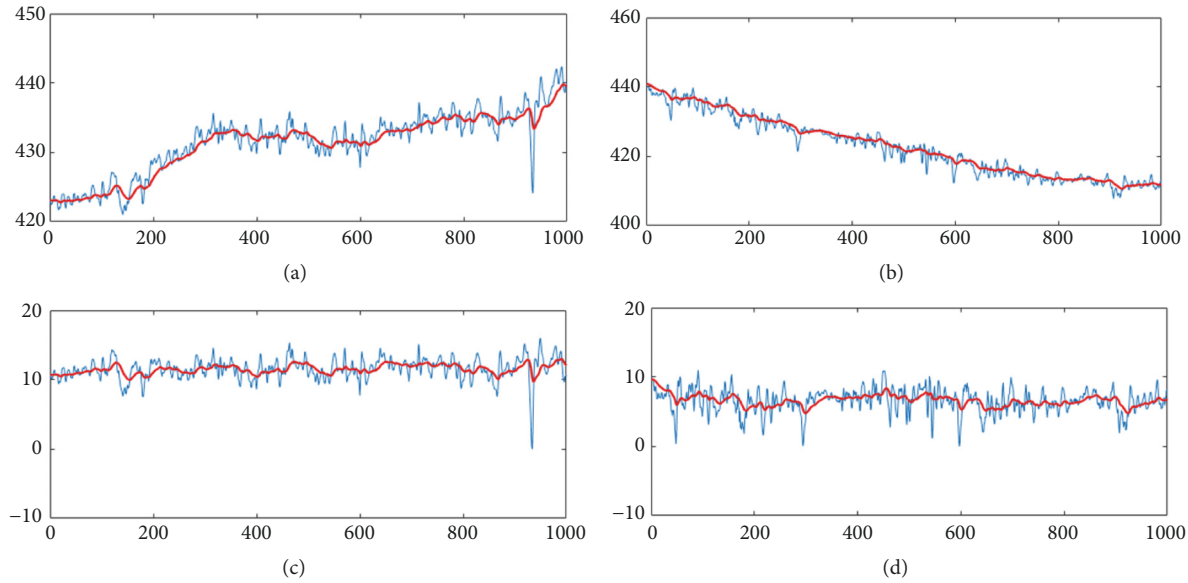

Figure 4: Examples of pavement 3D data rectification: (a) and (b) the original transverse profile and longitudinal profile; (c) and (d) the corresponding transverse profile and longitudinal profile.

Table 1: Composition of the SMFB.

Filter No.	Filter size	σ	θ
1-13	21×21	3	-90°,-75°,-60°,..., 90°
14-26	21×21	5	-90°,-75°,-60°,..., 90°
27-39	31×31	7	-90°,-75°,-60°,..., 90°
40-52	31×31	9	-90°,-75°,-60°,..., 90°

$$r^*(p) = \max r_i(p;\sigma,\theta) \tag{7}$$

$$R^*(p) = \begin{cases} 1 & if\ r^*(p) > thres \\ 0 & otherwise \end{cases} \tag{8}$$

where p denotes a pixel located at (x, y); $V(p)$ denotes the preprocessed 3D pavement data; $k_i(\sigma,\theta)$ denotes the i^{th} steerable filter in SMFB with parameters σ, θ; $r_i(p;\sigma,\theta)$ denotes the response based on convolutional output over k_i and $V(p)$. $r^*(p)$ denotes the maximum response; and $R^*(p)$ denotes the binary crack map by thresholding implement.

As illustrated in Figure 6, crack saliency maps are generated after implementing SMFB. Due to pavement texture, some noncrack pixels have high responses, resulting in false-positive errors. In addition, some crack pixels have low or even zero response, resulting in crack discontinuity and false-negative errors. Thus, additional procedure is needed to improve the detection accuracy.

2.3. Tensor Voting. Tensor voting (TV) is a perceptual grouping method proposed by Guy and Medioni [29]. In computer vision, TV is widely utilized to infer curvilinear structures [30], locally link the corrupted data [31], and extract the lines and curves from noisy images [32]. It is highly possible that some cracks have weak responses to the SMFB due to various reasons. Consequently, some cracks may be detected as discontinued fragments. In the paper, TV is adopted to enhance connections between crack fragments.

A second-order symmetric positive semidefinite tensor T is associated with each pixel in the crack saliency maps. T is mapped to a matrix $(a_{ij})_{2\times2}$, whose eigenvalues are $\lambda_1 \geq \lambda_2 \geq 0$, and corresponding eigenvectors are $\vec{e}_1$ and $\vec{e}_2$. Thereby the tensor can be deposed as follows:

$$\begin{aligned} T &= \lambda_1 \vec{e}_1 \vec{e}_1^{\,T} + \lambda_2 \vec{e}_2 \vec{e}_2^{\,T} \\ &= (\lambda_1 - \lambda_2)\vec{e}_1 \vec{e}_1^{\,T} + \lambda_2 \left(\vec{e}_1 \vec{e}_1^{\,T} + \vec{e}_2 \vec{e}_2^{\,T}\right) \end{aligned} \tag{9}$$

The first term $(\lambda_1 - \lambda_2)\vec{e}_1 \vec{e}_1^{\,T}$ in (9) represents a stick tensor as an elongated ellipsoid and the second is called "ball tensor" as a circular disk. First, a ball voting is used to estimate the crack-curve orientation at each crack pixel from the crack saliency maps, that is, each detected crack pixel is initialized as a ball tensor $\left(\begin{smallmatrix} 1 & 0 \\ 0 & 1 \end{smallmatrix}\right)$, and noncrack pixels do not participate in voting. The ball voting is conducted by adding the fields generated by the stick tokens spanning 360° at regular intervals. In this way, the principal direction at each crack pixel is found, which is set as the orientation of the stick token. Then a stick voting is applied by means of casting the votes from each stick token to all the pixels (crack pixels and noncrack pixels). For stick voting, assuming that O is the origin location and P is the voting location as shown

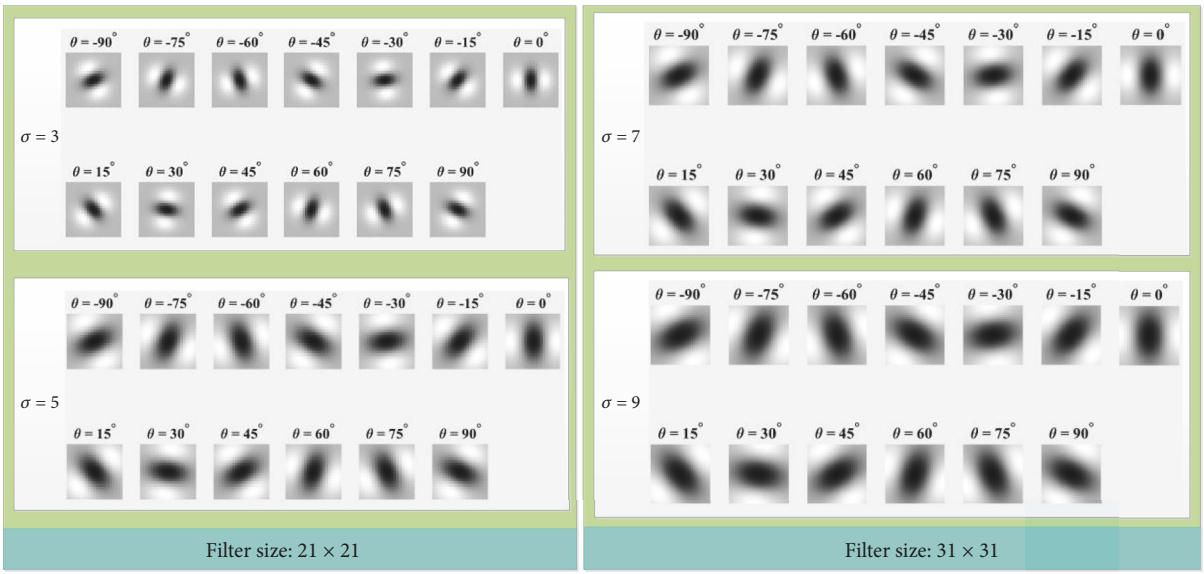

Figure 5: Steerable filters in SMFB.

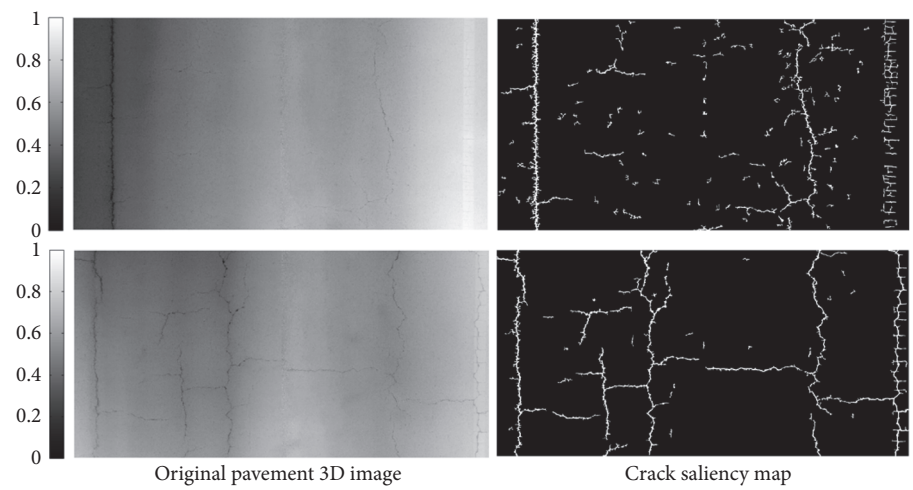

Figure 6: Examples of generated crack saliency maps.

in Figure 7, the voting field can be defined by using a decay function:

$$DF(s,k,\sigma) = e^{-((s^2+ck^2)/\sigma^2)} \tag{10}$$

where s is the arc length from this token to a target point in the voting field, k is the curvature, σ is the scale of voting, and c is a parameter controlling the degree of decay with curvature defined in (11) as

$$c = \frac{-16(\sigma - 1)\log(0.1)}{\pi^2} \tag{11}$$

As TV is used to enhance connections between crack fragments in this paper, after the stick voting stage, the dense tensor map is extracted as tensor voting result, which is different from the original tensor voting method presented in [33]. Lastly, the OR operation is executed on the dense tensor map and the crack saliency map. An overall illustration of our method is shown in Figure 8.

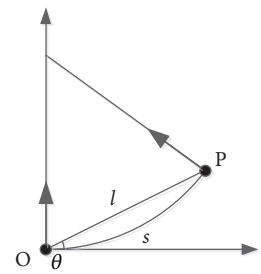

Figure 7: Votes cast by a stick tensor at the origin O.

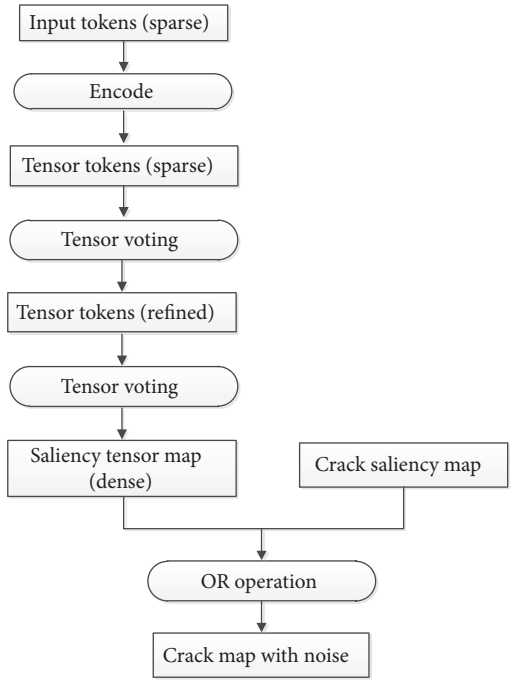

Figure 8: Overall TV approach.

After TV operation, missing parts of the detected cracks could be retrieved, resulting in enhanced continuity of cracks. Figure 9 provides typical examples of connecting discontinued parts using TV. In Figure 9, small fragments close to each other are linked together as a whole part, as highlighted by the dashed circles..

2.4. Postprocessing. After the TV operation, some noise pixels may still exist. The remaining noises can seriously affect the precision of crack detection. Hence, postprocessing is needed to further remove noises and refine the final detection output. In this paper, all connected components less than 1000 pixels are removed.

3. Experimental Results and Comparison

In this paper, precision, recall, and F-measure are used to evaluate the performance of the proposed method. Precision measures the exactness or fidelity of detection and segmentation, while recall describes the completeness of detection and segmentation. F-measure is the harmonic mean of precision and recall, where an F-measure reaches its best value at 1 and worst at 0. The definitions of precision, recall, and F-measure are shown in

$$Precision = \frac{TP}{TP + FP} \tag{12}$$

$$Recall = \frac{TP}{TP + FN} \tag{13}$$

$$F\text{-}measure = \frac{2 \times Precision \times Recall}{Precision + Recall} \tag{14}$$

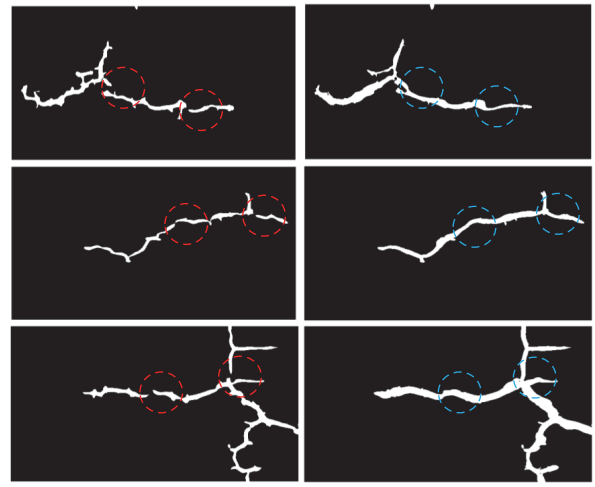

Figure 9: Examples of TV approach: the size of each patch is 700 × 300 pixel^2. The patches in the left column are cropped from the crack saliency maps; the patches in the right column are cropped from the results of TV operation.

In (12) and (13), *TP* denotes true positives; that is, pixels labeled as crack pixels in the ground truth are correctly recognized as crack pixels; *FP* denotes false positives; that is, pixels labeled as noncrack pixels in the ground truth are incorrectly recognized as crack pixels; *FN* represents false negatives; that is, pixels labeled as crack pixels in the ground truth are incorrectly detected as noncrack pixels. The ground truths of cracks were obtained by two steps: at the first step, crack maps were generated automatically by applying method proposed by Zhang [34]; at the second step, manual labeling was used to refine the crack maps provided by the first step. A pixel-to-pixel comparison is conducted during the evaluation.

A test data set consisting of two hundred 3D pavement images is selected to evaluate the proposed method. This test set covers images from different road sections, various lighting conditions (i.e., daylight and nightlight), and diverse severities of cracks (i.e., low-level or no crack, medium-level crack, and high-level crack). The computer hardware used for experiments is summarized as follows: Intel Core i7-6700T, 3.00 GHz CPU, and 32 GB RAM. All algorithms are implemented in MATLAB platform. Figure 10 presents some typical detection results using the testing images. As shown in Figure 10, the proposed method can detect cracks with varying widths, severity levels and contexts. In addition, typical false-positive and false-negative errors are shown within the dashed rectangles in Figure 10(b) and within the dashed circles in Figure 10(d), respectively.

Accordingly, the precisions and recalls for all the selected images are illustrated in Figure 11. The precision fluctuates between 84.00% and 97.00%, and the average precision is 88.38%, while the recalls range from 85.00% to 99.00%, and the average recall is 93.15%. In addition, the F-measure is between 85.00% and 97.00%, and the average F-measure is 90.68%.

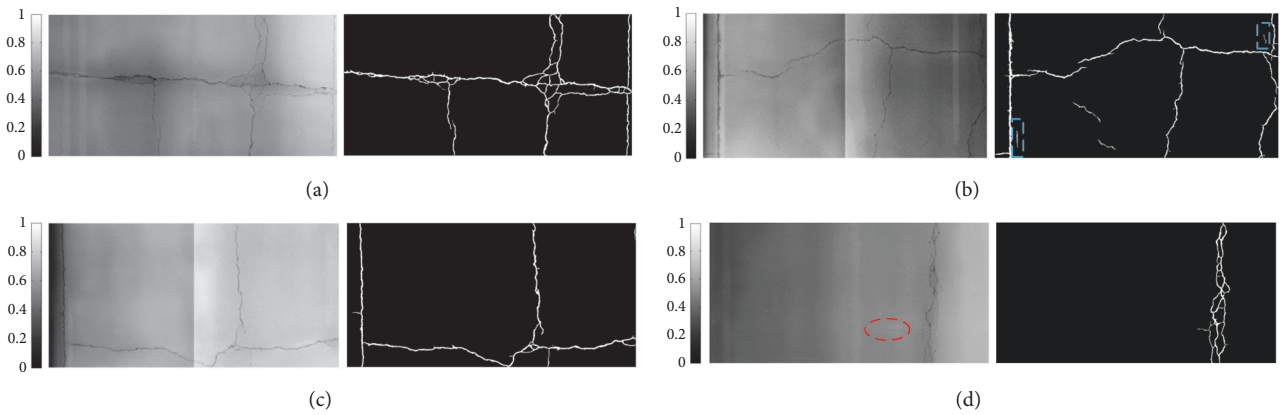

Figure 10: Experimentation results.

Table 2: Performance comparison of different methods.

Authors	Method	Precision	Recall	F-measure
Ouma and Hahn [3]	A triple-Transform	91.25%	80.42%	85.49%
Zou and Cao [18]	CrackTree	79%	92%	85%
Shuai and Yang [35]	Steerable Matched Filter	92.6%	85.1%	88.7%
-	Proposed method	**88.38**%	**93.15**%	**90.68**%

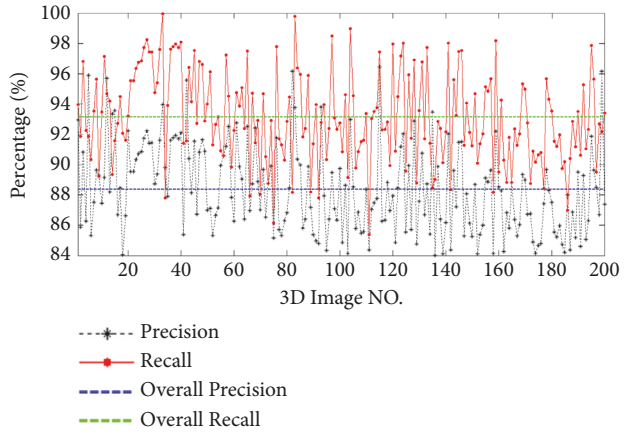

Figure 11: Precisions and recalls for 200 selected 3D images.

Many research works reported the performance of their methods for crack segmentation, as listed in Table 2, which demonstrates that the proposed method in this paper has a higher performance than those using other methods. It is acknowledged that the same set of images/data should be used to compare all methods, judge their performance, and estimate their potential. That requires direct access to both dataset and programs/codes/algorithms. Further efforts taken by different related research agencies are needed to create a benchmark dataset and form a comparison protocol.

4. Conclusions and Future Work

Automated pavement crack survey has drawn more and more attentions from both researchers and transportation agencies. This article proposed a novel method for segmenting crack maps based on 3D pavement images. The proposed method implements the SMFB operation, Tensor Voting, and preprocessing as well as postprocessing procedures in a specific order to detect cracks from 3D pavement images.

The experiment using 200 testing images demonstrated that the proposed method can achieve a high level of detection efficiency, quantified as average precision 88.38%, average recall 93.15%, and average F-measure 90.68%. The average precision was slightly lower than the average recall, implying that some noncrack pixels were incorrectly detected as crack pixels. A possible reason is that the edges of some pavement markings present height differences similar to those occurred at cracking area. The proposed method used the same set of fixed parameters to yield similar detection accuracies for all 200 testing images, implying that the proposed method has achieved an efficient generalization over varying cracks on 3D pavement surfaces.

Although the proposed method is efficient in detecting pavement cracks, it still needs to consume roughly 10.3s per image due to expensive computations primarily introduced by TV. In the future, parallel computing techniques may be considered to optimize the processing speed.

Data Availability

All of the data related to this paper is available for peer researchers to validate.

Conflicts of Interest

The authors declare that there are no conflicts of interest regarding the publication of this paper.

Acknowledgments

The authors would like to thank Dr. Kelvin C. P. Wang' s team for providing pavement 3D data. Funding for this research was supported by the National Natural Science Foundation of China (Grants nos. U1534203 and 51478398). The authors gratefully acknowledge the support.

References

[1] K. Gopalakrishnan, S. K. Khaitan, A. Choudhary, and A. Agrawal, "Deep convolutional neural networks with transfer learning for computer vision-based data-driven pavement distress detection," *Construction and Building Materials*, vol. 157, pp. 322–330, 2017.

[2] N.-D. Hoang and Q.-L. Nguyen, "A novel method for asphalt pavement crack classification based on image processing and machine learning," *Engineering with Computers*, 2018.

[3] Y. O. Ouma and M. Hahn, "Wavelet-morphology based detection of incipient linear cracks in asphalt pavements from RGB camera imagery and classification using circular Radon transform," *Advanced Engineering Informatics*, vol. 30, no. 3, pp. 481–499, 2016.

[4] N.-D. Hoang and Q.-L. Nguyen, "Automatic recognition of asphalt pavement cracks based on image processing and machine learning approaches: a comparative study on classifier performance," *Mathematical Problems in Engineering*, vol. 2018, Article ID 290498, 16 pages, 2018.

[5] M. Gavilán, D. Balcones, O. Marcos et al., "Adaptive road crack detection system by pavement classification," *Sensors*, vol. 11, p. 9628, 2011.

[6] C. Koch and I. Brilakis, "Pothole detection in asphalt pavement images," *Advanced Engineering Informatics*, vol. 25, no. 3, pp. 507–515, 2011.

[7] A. Mancini, E. S. Malinverni, E. Frontoni, and P. Zingaretti, "Road pavement crack automatic detection by MMS images," in *Proceedings of the 2013 21st Mediterranean Conference on Control and Automation, MED 2013*, pp. 1589–1596, June 2013.

[8] Y. Tsai, C. Jiang, and Z. Wang, "Pavement crack detection using high-resolution 3D line laser imaging technology," in *Proceedings of the 7th RILEM International Conference on Cracking in Pavements: Mechanisms, Modeling, Testing, Detection and Prevention Case Histories*, A. Scarpas, N. Kringos, and I. Al-Qadi, Eds., Springer, Dordrecht, Netherlands, 2012.

[9] A. Zhang, K. C. P. Wang, B. Li et al., "Automated pixel-level pavement crack detection on 3D asphalt surfaces using a deep-learning network," *Computer–aided Civil & Infrastructure Engineering*, 2017.

[10] J. Chang, K. Chang, and D. Chen, *Application of 3D Laser Scanning on Measuring Pavement Roughness*, 2006.

[11] J. L. Vilaça, J. C. Fonseca, A. C. M. Pinho, and E. Freitas, "3D surface profile equipment for the characterization of the pavement texture – TexScan," *Mechatronics*, vol. 20, no. 6, pp. 674–685, 2010.

[12] Q. Li, M. Yao, X. Yao et al., "A real-time 3D scanning system for pavement rutting and pothole detections," *SPIE Optical Engineering + Applications*, 2009.

[13] J. Laurent, D. Lefebvre, and E. Samson, *Development of a New 3D Transverse Laser Profiling System for the Automatic Measurement of Road Cracks*, 2008.

[14] F.-A. Moreno, J. Gonzalez-Jimenez, J.-L. Blanco, and A. Esteban, "An instrumented vehicle for efficient and accurate 3d mapping of roads," *Computer-Aided Civil and Infrastructure Engineering*, vol. 28, no. 6, pp. 403–419, 2013.

[15] K. C. P. Wang, L. LI, W. Luo, and A. Larkin, "Potential measurement of pavement surface texture based on three-dimensional image data," in *Proceedings of the Transportation Research Board 91st Annual Meeting*, 2012.

[16] W. Luo, K. C. R. Wang, L. Li, Q. J. Li, and M. Moravec, "Surface drainage evaluation for rigid pavements using an inertial measurement unit and 1-mm three-dimensional texture data," *Transportation Research Record Journal of the Transportation Research Board*, vol. 2457, pp. 121–128, 2014.

[17] A. Zhang, K. C. P. Wang, B. Li et al., "Automated pixel-level pavement crack detection on 3D asphalt surfaces using a deep-learning network: pixel-level pavement crack detection on 3D asphalt surfaces," *Computer-Aided Civil and Infrastructure Engineering*, vol. 32, no. 10, pp. 805–819, 2017.

[18] Q. Zou, Y. Cao, Q. Li, Q. Mao, and S. Wang, "CrackTree: automatic crack detection from pavement images," *Pattern Recognition Letters*, vol. 33, no. 3, pp. 227–238, 2012.

[19] H. D. Cheng, X. J. Shi, and C. Glazier, "Real-time image thresholding based on sample space reduction and interpolation approach," *Journal of Computing in Civil Engineering*, vol. 17, no. 4, pp. 264–272, 2003.

[20] H. Oliveira and P. L. Correia, "Automatic road crack segmentation using entropy and image dynamic thresholding," in *Proceedings of the 17th European Signal Processing Conference*, pp. 622–626, August 2009.

[21] Y. Maode, B. Shaobo, X. Kun, and H. Yuyao, "Pavement crack detection and analysis for high-grade highway," in *Proceedings of the 8th International Conference on Electronic Measurement and Instruments*, 4-552, 4-548 pages, 2007.

[22] A. Ayenu-Prah and N. Attoh-Okine, "Evaluating pavement cracks with bidimensional empirical mode decomposition," *EURASIP Journal on Advances in Signal Processing*, vol. 2008, Article ID 861701, 2008.

[23] J. Zhou, P. S. Huang, and F. P. Chiang, "Wavelet-based pavement distress detection and evaluation," *Optical Engineering*, vol. 45, pp. 409–411, 2003.

[24] M. S. Kaseko, Z.-P. Lo, and S. G. Ritchie, "Comparison of traditional and neural classifiers for pavement-crack detection," *Journal of Transportation Engineering*, vol. 120, no. 4, pp. 552–569, 1994.

[25] W. T. Freeman and E. H. Adelson, "The design and use of steerable filters," *IEEE Transactions on Pattern Analysis and Machine Intelligence*, vol. 13, no. 9, pp. 891–906, 1991.

[26] M. Jacob and M. Unser, "Design of steerable filters for feature detection using Canny-like criteria," *IEEE Transactions on Pattern Analysis and Machine Intelligence*, vol. 26, no. 8, pp. 1007–1019, 2004.

[27] S. Li, Y. Cao, and H. Cai, "Automatic pavement-crack detection and segmentation based on steerable matched filtering and an active contour model," *Journal of Computing in Civil Engineering*, vol. 31, Article ID 04017045, 2017.

[28] S. Mukherjee and S. T. Acton, "Oriented filters for vessel contrast enhancement with local directional evidence," in *Proceedings of the 12th IEEE International Symposium on Biomedical Imaging, ISBI 2015*, pp. 503–506, April 2015.

[29] G. Guy and G. Medioni, "Inference of surfaces, 3D curves, and junctions from sparse, noisy, 3D data," in *Proceedings of the*

International Symposium on Computer Vision, 1995, pp. 599–604, 1997.

[30] N. Strokina, T. Kurakina, T. Eerola et al., *Detection of Curvilinear Structures by Tensor Voting Applied to Fiber Characterization*, Springer, Berlin, Germany, 2013.

[31] L. Risser, F. Plouraboué, and X. Descombes, "Gap filling of 3-D microvascular networks by tensor voting," *IEEE Transactions on Medical Imaging*, vol. 27, no. 5, pp. 674–687, 2008.

[32] R. Moreno, L. Pizarro, B. Burgeth, J. Weickert, M. A. Garcia, and D. Puig, "Adaptation of tensor voting to image structure estimation," *Mathematics and Visualization*, no. 202519, pp. 29–50, 2012.

[33] G. Medioni, C. K. Tang, and M. S. Lee, "Tensor voting: theory and applications," in *Proceedings of The Right Format of Internet Advertising (Rfia)*, vol. 34, pp. 1482–1495, 2000.

[34] A. Zhang, K. C. P. Wang, R. Ji, and Q. J. Li, "Efficient system of cracking-detection algorithms with 1-mm 3D-surface models and performance measures," *Journal of Computing in Civil Engineering*, vol. 30, Article ID 04016020, 2016.

[35] S. Li, Y. Cao, and H. Cai, "Automatic pavement-crack detection and segmentation based on steerable matched filtering and an active contour model," *Journal of Computing in Civil Engineering*, vol. 31, no. 5, 2017.